CIRP Journal of Manufacturing Science and Technology 55 (2024) 333–346

Contents lists available at ScienceDirect

CIRP Journal of Manufacturing Science and Technology

journal homepage: www.elsevier.com/locate/cirpj

Full Length Article

Hybrid FE-ML model for turning of 42CrMo4 steel

Sampsa Vili Antero Laakso *, Andrey Mityakov, Tom Niinimäki, Kandice Suane Barros Ribeiro, Wallace Moreira Bessa

University of Turku, Faculty of Technology, Department of Mechanical and Materials Engineering, Joukahaisenkatu 3, Turku, 20520, Southwest Finland, Finland

ARTICLE INFO

Keywords:
Hybrid modelling
FEM
CEL
Machine learning
Deep neural networks
Machining
Turning
Cutting force
Simulation
42CrMo4 steel
Cubic boron nitride

ABSTRACT

Metal cutting processes contribute significant share of the added value of industrial products. The need for machining has grown exponentially with increasing demands for quality and accuracy, and despite of more than a century of research in the field, there are no reliable and accurate models that describe all the physical phenomena needed to optimize the machining processes. The scientific community has begun to explore hybrid methods instead of expanding the capabilities of individual modelling schemes, which has been more efficient than efficacious direction. Following this trend, we propose a hybrid finite element — machine learning method (FEML) for modelling metal cutting. The advantages of the FEML method are reduced need for experimental data, reduced computational time and improved prediction accuracy. This paper describes the FEML model, which uses a Coupled Eulerian Lagrangian (CEL) formulation and deep neural networks (DNN) from the TensorFlow Python library. The machining experiments include forces, chip morphology and surface roughness. The experimental data was divided into training dataset and validation dataset to confirm the model predictions outside the experimental data range. The hybrid FEML model outperformed the DNN and FEM models independently, by reducing the computational time, improving the average prediction error from 23% to 13% and reduced the need for experimental data by half.

1. Introduction

Sustainable and cost-efficient production requires optimization of the individual processes. A comprehensive understanding of the process physics and the effects of the process parameters on the outputs are prerequisites for the optimization. The process outputs in metal cutting, such as forces, chip formation, heat, and surface roughness, have non-linear behaviour as a function of process control parameters, like cutting speed, feed, and depth of cut. Furthermore, the underlying physics of metal cutting involves complex material behaviour where the properties change as a function of strain, strain rate and temperature. Due to that complexity, analytical modelling of metal cutting is unfeasible. However, numerical modelling, especially finite element method (FEM), has the potential to overcome the issues with complexity.

Despite that FEM models have steadily improved accuracy and simulation performance, they are still computationally expensive due to the non-linearities in the material model, coupled nature of the mechanical and thermal behaviour and the large deformations that require either a fine mesh or remeshing. Furthermore, creating a material model for the FEM simulations requires significant expertise and rigorous materials testing. Researchers have proposed different material modelling paradigms for FEM, which include complex physical testing of the materials, or inverse modelling the material behaviour from machining experiments. There are multiple inverse methods, but one of the most straightforward is response surface method, where the effect of each FEM model parameter is approximated with a polynomial. The output is then compared to experimental values, and the parameters that minimize the root mean squared error are chosen. Due to these challenges, several researchers have proposed machine learning (ML) as an alternative approach. Consequently, there are numerous implementations of ANNs in machining problems, e.g., cutting force prediction in ultrasonic milling [1], tool wear prediction in turning of Inconel 718 [2] and predicting the cutting force and surface roughness in milling of metal matrix composite [3].

Machine learning does not require in-depth expertise in materials, machining or even programming, and despite that, the models are able to reproduce the effects of the phenomena within the given training dataset, emphasizing the word within. ML methods, like any other regression models, can predict the behaviour well by interpolating the given datapoints and extract their interconnectedness, but the model performance decreases rapidly when the prediction is extrapolated outside of the peripheral boundaries of a given training dataset. Moreover, ML based methods require large training datasets, which are expensive

* Corresponding author.
E-mail address: sampsa.laakso@utu.fi (S.V.A. Laakso).

https://doi.org/10.1016/j.cirpj.2024.10.003
Received 16 July 2024; Received in revised form 3 October 2024; Accepted 6 October 2024
Available online 24 October 2024

to produce unless extracted directly from the manufacturing system using IoT/Industry 4.0 or other smart monitoring systems. The bottleneck appears to be the considerable number of experiments needed for both, ML and FEM.

Our approach is to use a minimum number of experiments to train the ML model and to use those same experiments for calibrating the FEM model. Henceforth, we can use the FEM results to expand the training dataset beyond the original experimental dataset. This combines the strengths of both methods, the computationally efficient interpolation capabilities of ML and accurate, although expensive FEM simulations for expanding the data domain, while minimizing the need for machining experiments.

Our model uses deep neural networks (DNN) for the machine learning algorithm, Coupled Eulerian Lagrangian (CEL) formulation for the FEM model and machining experiments for the training and verification datasets. The DNN is built with TensorFlow library available for Anaconda Python distribution. The CEL model is built with the commercial FEM package Abaqus CAE. The first application of CEL on machining was done by Ducobu et al. [4] in 2016, and later used extensively by Agmell et al. [5,6]. Guo and Wen [7] developed a hybrid numerical model for cutting by applying an analytical model for chip stagnation into an arbitrary Lagrangian–Eulerian (ALE) FEM model. The model is able to capture the intended chip shape and stagnation effects. Currently FEM models are capable of capturing the same effect using friction models and adaptive remeshing, to avoid element deletion. The CEL model used in this research has the advantage of avoiding even the adaptive remeshing and the model performance regarding computational time in 3D problems is better than with Lagrangian formulation.

There are multiple approaches to hybrid modelling: In civil engineering, the HYMOD approach was proposed by Markou and Papadrakakis [8] which used multiple FEM formulations to efficiently simulate reinforced concrete structures. Contact problems benefit from hybrid methods by combining boundary element method (BEM) with FEM in applicable roughness scales [9]. DNN based material models have been demonstrated in FEM [10] and even microstructural variations within heterogeneous materials can be solved using FEM and DNNs [11].

In the field of manufacturing research, hybrid methods using FEM and ML have been used for predicting micro-scale forces in grinding [12]. Li et al. [13] present one of the first hybrid modelling methods for machining with single point tools. Their approach uses Oxley's parallel sided shear zone theory and neural networks. The analytical model is used to predict the mechanical phenomena, forces, temperatures and chip morphology. Those variables, together with tool and coolant data, are used as an input for the neural networks. The model uses separate neural network for each predicted outcome, i.e. tool wear, surface roughness and chip breakability. The neural networks are trained with experimental data. The model prediction accuracy varies between 5%–20%. Their experimental verification, however, has only one variable, the cutting speed.

Jawahir et al. [14] in 2003 discuss the broader view of hybrid modelling for optimized machining and its applications in intelligent manufacturing systems. The existing methods are listed as analytical techniques, numerical modelling, artificial intelligence (AI) and fuzzy logic based methods. They highlight the need, especially for hybrid models, for predicting the machining performance metrics instead of individual, method dependent outputs. They considered the characteristic issues of each method; FEM models' prediction outputs are not equal to machining performance prediction values and FEM models need accurate material data. Empirical models are valid only within restricted parameter space and need considerable experimental testing effort. AI and fuzzy models require large teaching datasets.

Our approach has an added benefit in the context on intelligent control, because the machining databases for hybrid FEML modelling do not need to be complete, as the underlaying DNN can predict the missing parameters and FEM can improve the prediction accuracy if necessary. Therefore, the database can be compiled from multiple sources even if the dataset is incomplete. Jawahir et al. [15] revisit the themes of the 2003 paper, reviewing the new developments. They conclude that regardless the developments in the methods, none of the modelling techniques are accurate or reliable enough to be used for optimization in industry.

Ahilan et al. [16] present a hybrid decision making tools for CNC turning quality. Their hybrid method is to train artificial neural network (ANN) with either backpropagation, genetic algorithm or particle swarm optimization (PSO). The models are used to predict power consumption and surface roughness at different process parameters values, which were varied for cutting speed, feed, cutting depth and nose radius. The ANN trained with PSO had the best prediction performance, showing roughly less than 10% error in overall results. Their results gave us confidence on implementing our idea of hybrid FEML, because surface roughness is notoriously difficult to predict, but their ANN did that with reasonable accuracy.

Pérez-Salinas et al. [17] analysed orthogonal cutting of Inconel 718. Their results show correlation between flank wear and increased oscillations in shear force. If these oscillations can be captured from FEM simulations, it will potentially provide a path to model surface roughness based on the FEM simulations without spending excessive resources on the mesh size. Following that thought, kinematic modelling accompanied with the chip formation mechanics shows promise, as shown by Lazkano et al. [18]. They modelled surface topography using kinematics of a milling tool complemented with experimentally determined stochastic effects of chip formation, material defects and vibrations. Including the stochastic effect to the kinematic model improved the model accuracy by 27%–73%.

Aldekoa et al. [19] investigate tool wear in broaching by monitoring the servomotor power. The correlation between the torque signal acquired from the servomotor power and tool wear is done with Support Vector Machine Regressor (SVMR), K-Nearest Neighbours Regressor (KNNR), and Random Forest Regressor (RFR). All regression models performed well and RFR had the highest accuracy.

Schoop et al. 2019 [20] use a multi-domain hybrid model coupled with experimental input to predict surface integrity in machining. The domains in the model are elastic, plastic, thermal and thermodynamic domains. Thermal model is based on frictional heating calculated using modified Bessel equations, the plastic domain uses Oxley's slip line theory for polishing and elastic domain is based on Hertz's theory explaining elastic contact. Thermodynamic domain is used for modelling phenomena such as dynamic recrystallization and phase changes. Although their model gives reasonably good prediction compared to the experiment ($\pm 10\%$), they used only one set of cutting conditions in their error evaluation and the model has the same inherent flaws as any 2D based modelling scheme. In their more recent work, Schoop et al. 2022 [21] address the limitations of the 2D model, where they investigate residual stresses (RS) in machining by combining 2D analytical model and using in-situ Digital Image Correlation (DIC) for measuring the strain fields. The normal pressure was determined from the DIC displacement fields using Hertz's theory of elastic contact between cylinders on a plane in plane strain conditions. The 2D model is then projected to 3D by calculating the equivalent chip thickness along the tool nose radius and running the 2D model on different chip thicknesses. The model assumptions are reasonable and the inherent inaccuracies in the model are minor compared to the overall residual stress field on the machined surface. The comparison of the residual stress distributions calculated with the model shows decent agreement with measured RS distributions. Our future research objective is to include the surface integrity into our hybrid ML model, following similar methodologies as Schoop et al.

Shi et al. [22] modelled cryogenic coolants in machining using computational fluid dynamics (CFD) with FEM. The CFD model predicted the coefficients of heat transfer (CHT) between the liquid nitrogen spray

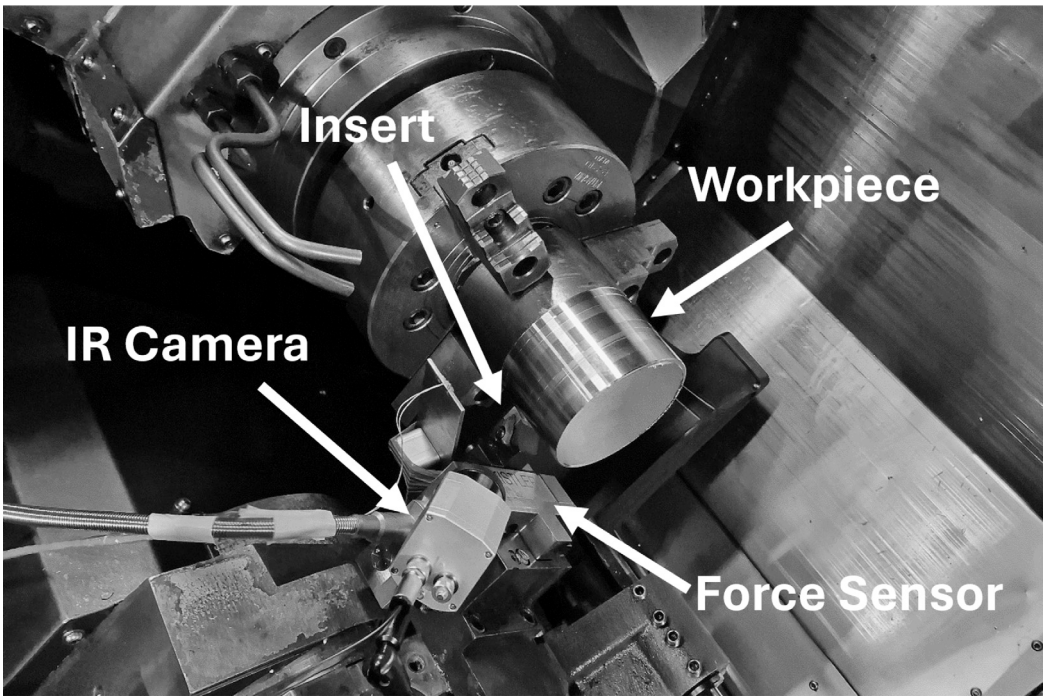

Fig. 1. The experiment setup on the NC lathe.

and the insert, workpiece, and chip. The predicted CHTs were used in the FEM model as thermal boundary conditions, so the CFD and FEM models were not coupled. The model predicted the chip temperature with 7% error and the cutting forces with −24% to 10% errors.

Reimer [23] did extensive experimental and modelling effort to predict surface integrity and fatigue life of forging dies after milling in a doctoral dissertation from 2019. The model uses ANN to predict the surface roughness, hardness and residual stresses caused by the milling process. The ANN output is checked against initial machining dataset and FEM results are used to improve the prediction. The fatigue life is predicted and optimized with genetic algorithm by adjusting the machining parameters. Although the accuracy of the model leaves room for improvement ($R = 0.725$), the modelling effort, scope and holistic approach are commendable. Our research concept was inspired by the work done by Dr Reimer.

Kurz et al. [24] review different hybrid modelling techniques within scientific computing. The review summarized the methods to Physics Informed Neural Networks (PINNs), Deep Learning with embedded physics simulation and Field Inversion and Machine Learning (FIML). Concluding remark points out that hybrid modelling is spreading in different fields in natural sciences and engineering.

The outcome of our literature review results to similar observation, there are numerous hybrid methods using analytical models with ANN even within the field of metal cutting research. However, there are only few papers with hybrid FE-ML methods. Furthermore, we did not find any previous publications that use 3D FEM, only one paper to use FEM with DNN, and only two papers using synthetic teaching data. However, some similarities with the hybrid FEML do exist. For example, Hashemitaheri et al. [25] produced training data with 2D Lagrangian FEM model for regression algorithms. Although the concept of synthetic data is similar, the extent of the data variables, model dimensions, work material, FEM formulation, ML approach are all different. Most notable difference is that their approach is only capable of predicting specific cutting forces and tool temperature. Another similar approach is done by Peng et al. [26] using 2D FEM for additional training data source for multilayered ANN for predicting cutting forces. The following research gaps were identified:

- No FEML implementations of three dimensional FEM.
- No FEML implementations of CEL formulation.
- No FEML implementations for 42CrMo4.
- No FEML implementations predicting surface roughness.
- No FEML implementations predicting chip thickness.

Therefore, it can be stated that the novelty of this work is using high-fidelity 3D FEM model using CEL formulation to generate synthetic training data for the DNN to complement experimental training data for predicting cutting forces, chip thickness and surface roughness in turning of 42CrMo4 steel with CBN insert. The objective of this paper is to demonstrate the capabilities of the hybrid FEML model and investigate if, and how much, the FEM results improve the DNN model accuracy outside of the experimental dataset range. The intended research outcomes are (a) to decrease the need for experiments, (b) to reduce computational time and (c) improve prediction accuracy.

2. Materials and methods

We performed machining tests with an NC lathe with maximum spindle speed of 3500 r/min and spindle power of 26 kW (Puma MX2500ST), which included force measurements (Kistler 9129AA) and thermal imaging (Optris PI640), as shown in Fig. 1. Although the emissivity factor of the IR camera was properly calibrated for both work material and insert by adjusting the emissivity while measuring the material surface temperature with contact thermocouple, we discarded the thermal imaging results because the temperatures of the workpiece, chips and insert interfered (overlapped) with each other and capturing any meaningful results would have required going through the measurement data frame by frame. Additionally chip thickness (digital vernier calliper) and surface roughness of the workpiece were measured with 3D microscope (Alicona Infinite Focus G6, shown in Fig. 2) after the experiments. The microscope objective was the 400 WD19, with vertical resolution set to 0.54 µm and a lateral resolution to 0.93 nm, which enable measuring radius down to 3 µm.

We created two datasets; one is used for the initial training dataset for the ML model and FEM model calibration, and the second dataset is used as verification dataset for the models. The first dataset is a 2-level full factorial with a centre point, where the centre point values

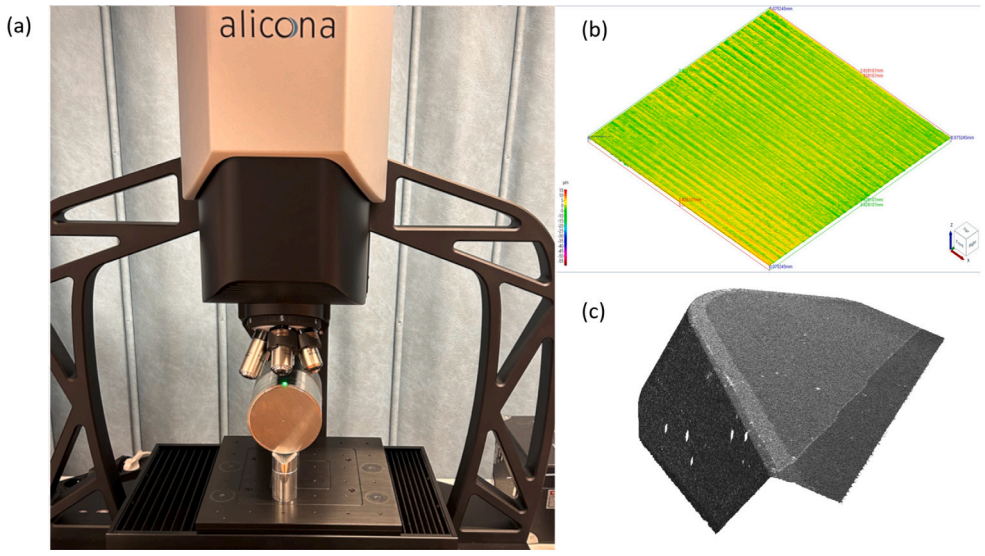

Fig. 2. (a) Alicona Infinite Focus G6 3D microscope, (b) workpiece surface topology, (c) 3D cutting edge profile of the CNB insert.

Fig. 3. The CBN insert.

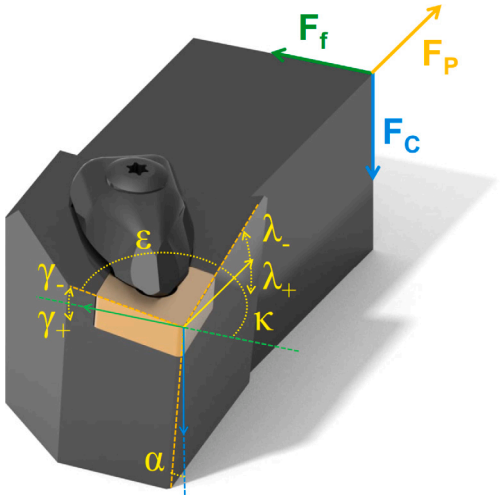

Fig. 4. The cutting tool angles and force components.

were chosen based on the tool manufacturer Seco tools' recommendation, and the low and high levels were scaled ±25% from the centre values, as in the Table 1. The second dataset added two levels to each parameter (Table 2), scaling the centre values with ±50%. In all, there are seventeen experiments with unique parameter combinations, and each combination was repeated three times, leading to total of 51 experiments.

Table 1
Design of experiments for the dataset 1: training dataset.

Test ID	v_c [m/min]	f [mm/rev]	a_p [mm]
A	225	0.125	0.5
B	135	0.125	0.5
C	225	0.075	0.5
D	135	0.075	0.5
E	180	0.100	0.4
F	225	0.125	0.3
G	135	0.125	0.3
H	225	0.075	0.3
I	135	0.075	0.3

Table 2
Design of experiments for the dataset 2: validation dataset.

Test ID	v_c [m/min]	f [mm/rev]	a_p [mm]
J	270	0.15	0.6
K	90	0.15	0.6
L	270	0.05	0.6
M	90	0.05	0.6
N	270	0.15	0.2
O	90	0.15	0.2
P	270	0.05	0.2
Q	90	0.05	0.2

Cutting length was selected for each datapoint so that the cutting time was exactly 10 s. Each datapoint was repeated three times to have elementary statistical confidence on the results. The workpiece was Ø120 mm round bar of Ovako 42CrMo4 steel in quenched and tempered state, which we measured with Innovatest Falcon 600, having nearly uniform hardness of 300 Vickers (HV1) across the cross section, with standard deviation of 9.6% in 20 sampled points. The 42CrMo4 was chosen because it has well defined QT-temperature–time hardness behaviour, therefore including hardness in future work with the same material will be easier. Seco CBN inserts, shown in Fig. 3 (CNGA120408S-01525-L1-B CH2540) were used in the experiments attached to a DCLNR2525M12-M type tool holder. The CH2540 grade consist of 65% CBN and the remainder is ceramic matrix. CBN grain size is bimodal, in which 1 μm grains are complemented with 15 μm grains added to the structure. The cutting tool angles for the setup are

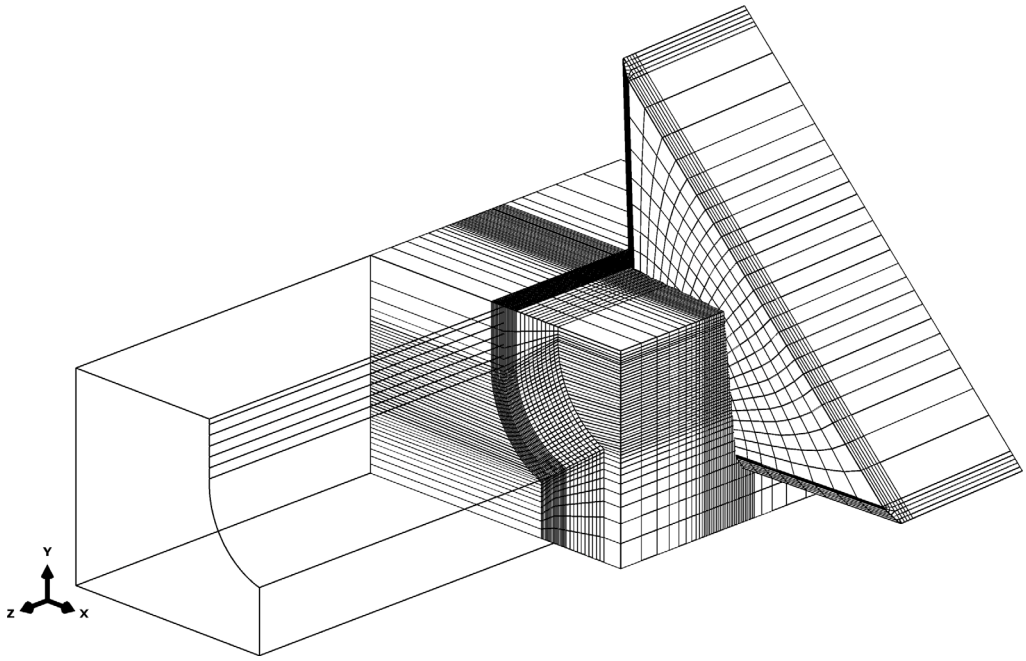

Fig. 5. The FEM model setup.

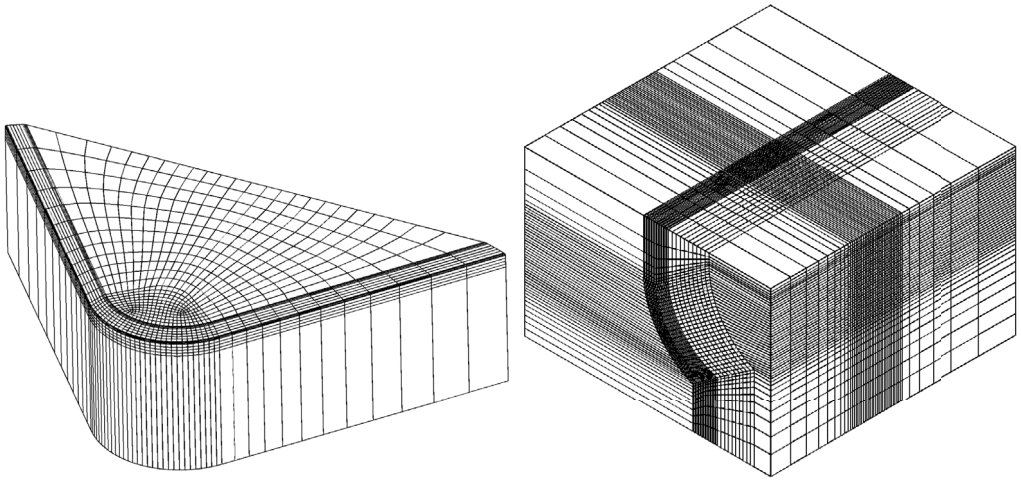

(a) Insert (b) Eulerian

Fig. 6. Mesh configuration in the FEM simulations (a) insert, (b) Eulerian.

95° for the cutting edge angle κ, −6° for rake angle γ and −6° for the inclination angle λ, as shown in Fig. 4. The flank angle α is equal to rake angle with N-type inserts. Wedge angle ϵ of the insert is 80° and nose radius is 0.8 mm and the tool cutting edge has 0.15 mm chamfer at 20° angle from the rake face. The cutting edge radius was measured to be 20 µm. Each datapoint was machined with a new cutting edge to eliminate the effect of wear. We investigated the inserts before and after the experiments, using the Alicona microscope (Fig. 2) and observed no measurable wear (see Fig. 2 c).

2.1. FEM model

We built the FEM model with Abaqus CAE, using Coupled Eulerian Lagrangian (CEL) formulation using linearized 3D representation of the round workpiece as shown in Fig. 5. The workpiece geometry was used to assign material inside the Eulerian space which interacts with the insert modelled with Lagrangian formulation. The material inside the Euler space was tracked using the Volume Fraction tool. The solver uses explicit time integration with dynamic coupled temperature–displacement. The simulation time is set to 0.001 s, leading to different cutting lengths depending on the cutting speed.

The insert was meshed (Fig. 6a) with 8-node thermally coupled brick elements with trilinear displacement and temperature (C3D8T) having minimum edge length of 0.01 mm and maximum edge length of 1 mm. The number of elements in the insert mesh is 6462. The Eulerian space (Fig. 6b) is meshed with 63 360 8-node thermally coupled linear Eulerian brick elements with reduced integration and hourglass control (EC3D8RT), having minimum edge length of 0.015 mm and maximum edge length of 2 mm. The minimum edge length was selected based on generalized rule of 5 to 10 elements to the direction of uncut chip thickness. The contact between the insert and the workpiece was set with penalty formulation Coulomb friction on tangential direction and hard contact on normal direction, heat generation using Abaqus default values and thermal conductance was set with pressure dependent

Table 3
Johnson-Cook model parameters.

A [MPa]	B [MPa]	C	n	m	T_{room} [K]	T_{melt} [K]
637	608	0.0241	0.135	0.09193	300	1720

Table 4
Material properties of 42CrMo4 and CBN.

Mechanical properties	42CrMo4	CBN
Young's Modulus [GPa]	219	652
Density [kg/m^3]	7850	3940
Poisson's ratio	0.3	0.27
Thermal Expansion [mm/mmK]	1.20E−05	5.20E−06

tabulated data from Rosochowska et al. [27]. The simulation model parameters were calibrated using the experiments. The cutting parameters in the simulations were selected corresponding to the test IDs A, E, I, which were used to calibrate the friction coefficient of the model and the flow stress model parameters if necessary. Three values were used for calibration of the friction coefficient. The output parameters, cutting forces and chip thickness are linearly correlated to the friction coefficient and the output parameters are extrapolated or interpolated to goal values (experimental results) and then corresponding friction coefficient value is selected. The friction coefficient was finally set to 0.760, that well corresponds to existing research literature on dry cutting. The cutting force and chip thickness errors were within the acceptance range after the friction calibration, so no further adjustment of the flow stress model parameters was needed. The CBN insert was modelled as elastic part with initial field for temperature set to 300 K and an encastré boundary condition was set on the non-contact free surfaces. Workpiece was modelled as elastic–plastic using Johnson-Cook flow stress model [28], shown in Eq. (1). The J-C parameters for 42CrMo4 were taken from Stampfer et al. [29], shown in Table 3.

$$\sigma_{flow} = (A + B\varepsilon^n)\left(1 - C ln\left(\frac{\dot{\varepsilon}}{\dot{\varepsilon}_{ref}}\right)\right)\left(1 - \left(\frac{T - T_{room}}{T_{melt} - T_{room}}\right)^m\right) \quad (1)$$

Thermomechanical properties of the CBN insert and 42CrMo4 workpiece are presented in Table 4. The 42CrMo4 values are from Ovako Steel material datasheet and CBN values from Agmell et al. [5]. The Eulerian space was set with 300 K initial temperature field, the inflow surface (normal to z-axis in Fig. 5) was set with velocity boundary condition corresponding to the cutting speed, and y- and x-direction movement was restricted with zero velocity boundary conditions on the bottom and back surfaces. An average simulation time was 40 h using IT Centre for Science Ltd. Puhti supercomputer nodes with Intel Xeon Gold 6230 processor with 16 cores and 2.1 GHz clock speed and a single NVidia V100 GPU acceleration. First the simulations A, E and I and then simulations J to Q were calculated parallel, therefore the real-world simulation time was only slightly over 80 h.

2.2. Machine learning model

The machine learning model we used in this work, utilizes Python libraries, specifically TensorFlow and Keras for model construction and training. TensorFlow is a library for deep neural networks (DNN). We chose DNN for our hybrid method over ANN because DNN's accuracy and computational efficiency is higher than ANN's in complex datasets [30]. DNNs contain more hidden layers that enable them to represent more complex relationships than ANNs [31]. DNN's neurons in the hidden layers have interconnections which further improve the predictive capabilities. DNNs are also computationally more efficient than ANNs regarding the training of the network. We used Keras Tuner for optimizing the hyperparameters. Scikit-learn, another Python library, was used for data preprocessing and performance metrics calculations. During this preprocessing phase, the MinMaxScaler was employed to rescale the dataset to adjust all values within the range 0, 1. This scaling ensures that each data point contributes equally to the model's training and facilitates an accurate and unbiased evaluation of model outputs. However, the MinMaxScaler is sensitive to outliers, which can distort the data range and subsequently affect the scaling [32].

The initial approach involved constructing simpler models and experimenting with various batch sizes. Once the optimal batch sizes were identified, the final tuning of the models was executed using Keras Tuner. Keras Tuner automatically selects optimal hyperparameters for neural network models by efficiently exploring the possible configurations and maximizing model performance through a systematic and guided search process [33]. The tuning specifically employed the Hyperband optimization algorithm. Developed by Li et al. [34] the Hyperband algorithm significantly improves tuning efficiency by strategically allocating computational resources and prematurely terminating the training of underperforming parameter sets. Different loss functions were tested during the tuning process, and the Huber loss function, developed by Peter Huber, 1964, [35] emerged as the most effective. This function combines the attributes of mean squared error and mean absolute error. It applies mean squared error to smaller errors to increase sensitivity and mean absolute error to larger errors to enhance robustness against outliers.

The model was trained with two datasets, the first containing only the experimental data, and second with added FEM results. The data was split to 20%–80% validation dataset and training dataset in both cases. While we trained the DNN with the experimental dataset, the depth of the model was allowed to vary between one and three hidden layers. Neuron counts in the input layer were tested between 5 and 20 to explore varying complexities, while those in the hidden layers were set between 10 and 30. Learning rates of 0.1 and 0.01 were chosen, and the delta parameter for the Huber loss function was adjusted between 0.7 and 1. In addition to these settings, hyperbolic tangent (tanh), Rectified Linear Unit (ReLU), and sigmoid were available as tuneable activation functions for the input and hidden layers, while the output layer was set with a linear activation function. The tuner finalized the following optimized DNN model parameters: The model features an input layer with ten neurons using a hyperbolic tangent activation function and a single hidden layer with 16 neurons, also activated by a hyperbolic tangent. The learning rate was optimized to 0.1, and the Huber loss function, with a delta setting of 0.8. The model's training was conducted over 125 epochs.

The extended dataset was complemented with surface roughness values modelled with the DNN, because the FEM prediction of surface roughness is not feasible without unreasonable computational resources. With more training data for the DNN model, the tuner configuration had 10 to 30 neurons in the input layer and 15 to 40 in each hidden layer, with the depth of the network varying from two to four layers. Tanh, ReLU, and sigmoid were selectable as activation functions for the input and hidden layers, while the output layer was set with a linear activation function. Learning rates of 0.01 and 0.001 were chosen, and the threshold for the Huber loss function was set between 0.5 and 1. The optimized parameters for model 2 include an input layer with 30 neurons using the rectified linear unit and two hidden layers: the first with 15 neurons using the hyperbolic tangent and the second with 24 neurons using the rectified linear unit. The learning rate was set at 0.01, and the Huber loss function delta was set at 0.9. The model underwent training over 250 epochs.

3. Results

3.1. Machining experiments

The machining experimental results are presented in Table 5. The values are averages of three measurements and the corresponding standard deviations are in the following columns denoted with sigma. The forces have relatively low standard deviation at 4%–8% in average. The chip thickness has higher deviation at 10% on average. The surface roughness values have the highest uncertainty with 16% average standard deviation.

Table 5
The forces, chip thickness and surface roughness from the cutting experiments, and corresponding standard deviations.

ID	F_P [N]	F_C [N]	F_f [N]	σ_{F_p} [N]	σ_{F_c} [N]	σ_{F_f} [N]	t_c [μm]	σ_{t_c} [μm]	r_a [μm]	σ_{r_a} [μm]
A	187.3	228.5	146.3	6.6	15.6	15.3	210	26.5	0.83	0.04
B	202.6	243.9	157.7	3.0	12.6	9.9	227	11.5	0.88	0.16
C	144.4	162.4	120.0	6.4	8.7	8.9	147	35.1	0.39	0.04
D	153.7	173.2	126.9	5.1	10.3	9.7	140	10.0	0.59	0.17
E	151.1	162.3	105.7	8.7	14.3	13.4	170	10.0	0.66	0.11
F	146.4	150.4	82.7	10.5	17.2	12.7	187	28.9	0.89	0.09
G	160.8	161.4	87.8	9.6	17.0	14.2	197	11.5	0.79	0.11
H	113.8	107.3	69.4	9.3	12.9	11.8	127	15.3	0.42	0.14
I	124.9	116.7	72.6	6.8	11.1	10.0	107	5.8	0.88	0.12
J	217.0	293.0	179.8	3.1	0.3	0.6	240	17.3	1.06	0.11
K	254.3	335.2	213.0	3.9	2.8	1.7	307	40.4	1.38	0.19
L	125.5	145.1	127.5	5.2	3.8	4.0	100	20.0	0.27	0.03
M	144.8	174.4	143.7	1.7	2.6	0.4	117	11.5	0.86	0.33
N	117.3	109.7	46.4	5.1	3.1	3.6	147	11.5	1.07	0.02
O	140.8	133.2	49.1	4.2	3.5	5.7	247	5.8	0.86	0.12
P	72.3	56.0	33.5	2.0	1.1	1.2	77	5.8	0.36	0.08
Q	86.5	74.1	37.2	3.3	1.6	2.4	93	5.8	2.15	0.40

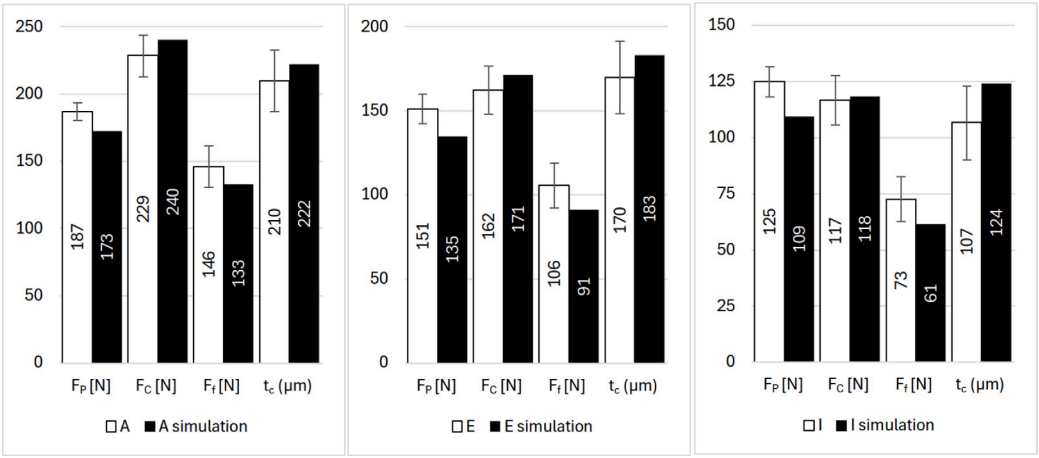

Fig. 7. FEM model output comparison against experiment IDs A, E, and I.

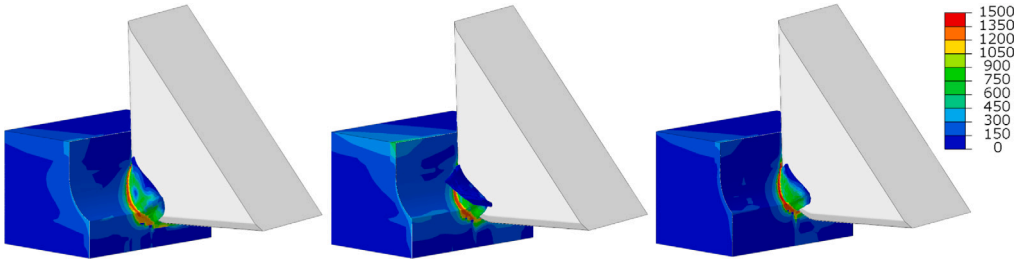

Fig. 8. FEM simulation output for IDs A, E, and I, from left to right.

3.2. FEM prediction results

The FEM model was calibrated to A, E and I experiments. The comparison of the calibrated FEM model against the experimental results is shown in Fig. 7. Average errors regarding the forces are from −13% to 4% and 10% for the chip thickness. Simulation output visualizations are shown in Fig. 8, where the colour-coding corresponds to Von Mises stresses (MPa).

The FEM model performance outside of the calibration dataset is crucial because the final hybrid model is reliant on the accuracy of the FEM model. Therefore, the FEM model error in parameter range J-Q is also evaluated, although this comparison was not used to modify the FEM or the ML models. The comparison to experiments is shown in Fig. 9 regarding the cutting forces and chip thickness. The forces have an average error between −4% to 11% and chip thickness has 10% average error compared to experimental results. In general, less than 10% errors in metal cutting FEM simulations have rarely been demonstrated in the field while using wide range of cutting parameters. Additionally, when considering the error magnitude, the experimental

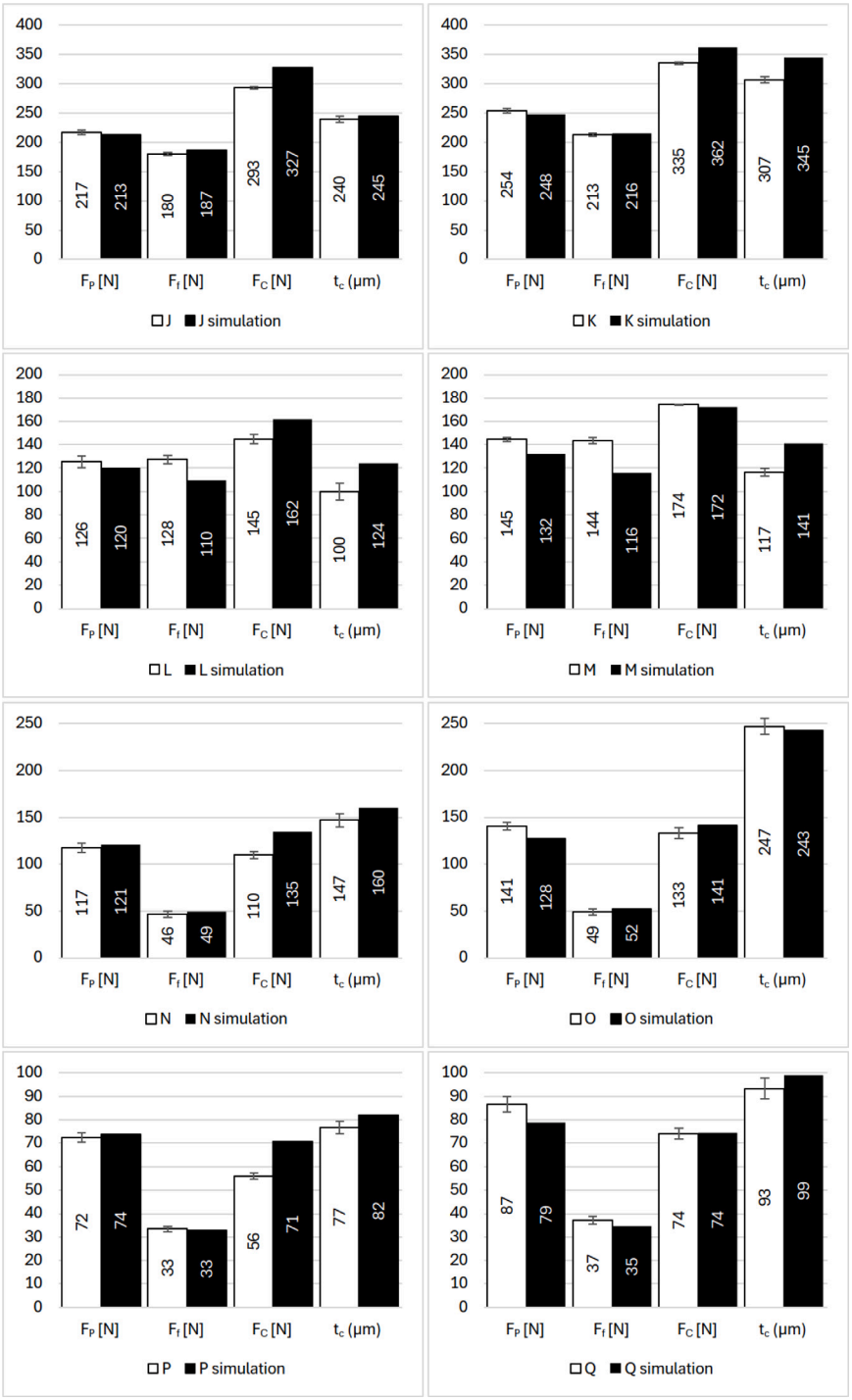

Fig. 9. FEM model output comparison against experiment IDs J-Q.

results have nearly as large standard deviation as the FEM error. Visualization of the simulations J-Q are shown in Fig. 10.

3.3. ML and hybrid FEML results

The ML and hybrid FEML model predictions are shown in Fig. 11 compared to the experimental results. The ML model with limited training dataset produced mean average error of 23% and R^2 is 0.43. The error is 6% for the labels A to I which were used for the training dataset and 42% for the validation dataset including labels J to Q. Maximum individual label error is 260% regarding the feed force prediction of the label O. Individual prediction errors for each label are given in Table 6. The hybrid FEML model average error is 13% for all labels and R^2 is 0.73, average error for the training dataset is

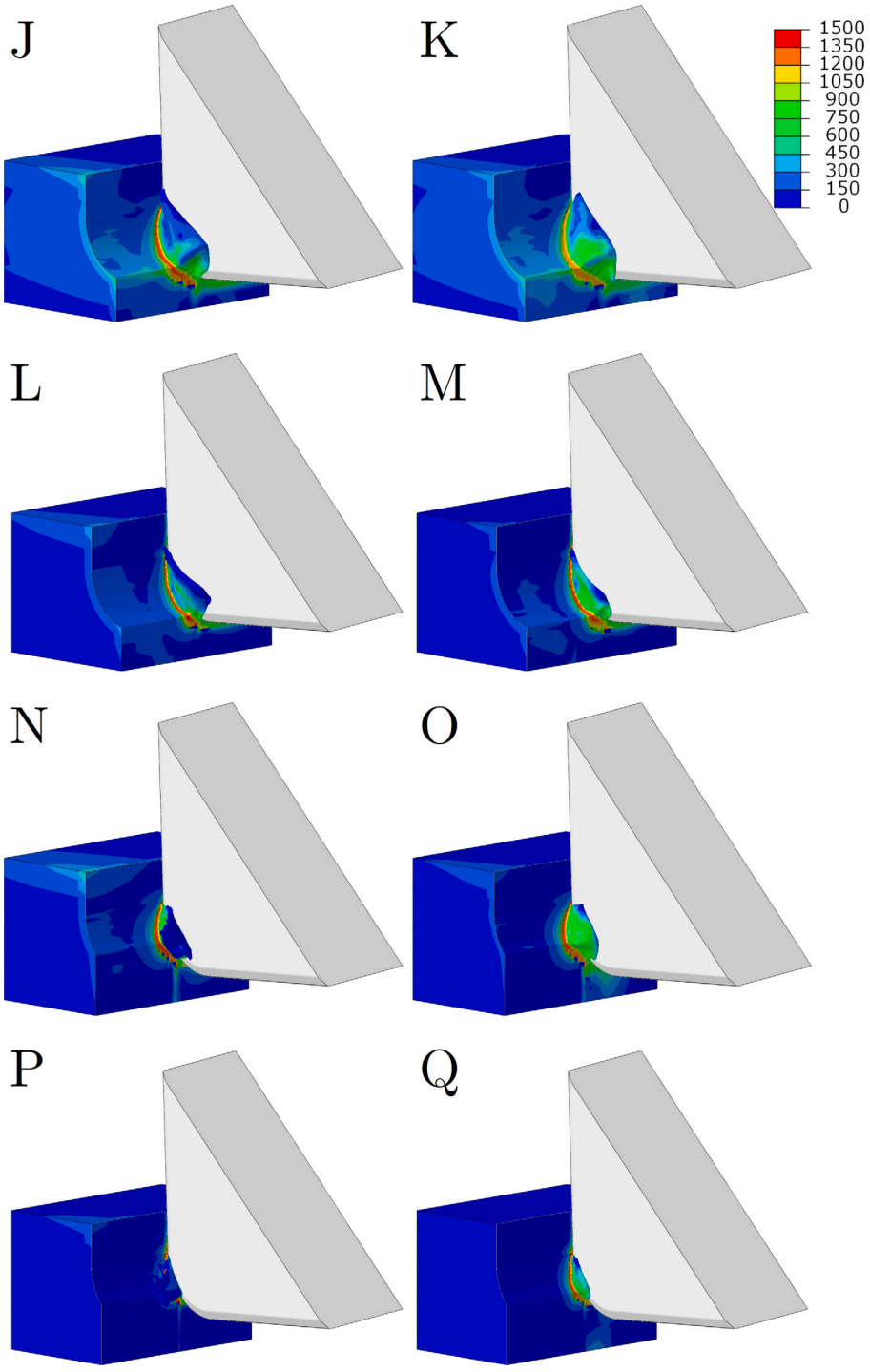

Fig. 10. FEM simulation output for IDs J-Q, from left to right and top down.

7% and 19% for the validation dataset. Maximum error of the hybrid FEML model is 77%, also for feed force, but for the label N. Error for all labels are shown in Table 7.

4. Discussion

The hybrid FEML model outperforms both the experiment driven DNN model and the FEM simulations. The average prediction error decreases with the hybrid FEML model to 13% from the ML model's 23%. The hybrid model benefits from the advantages of both methods, the powerful interpolation capabilities of the DNN and accurate extrapolation capabilities of the FEM model. Additionally, the experimental results can be used for multiple purposes: initial training dataset for the DNN model, calibration dataset for the FEM model and finally verification of the model performance. We observed a trend in the prediction errors, which tends to increase at the minimum and maximum boundary values of the process parameters, cutting speed, feed and cutting depth. The behaviour is common with DNN models, which can predict the outcomes only within the training dataset. The model errors can be associated to the size of the training data regarding the DNN. Increasing the number of the hidden layers would not improve the accuracy and would lead to overfitting. Only viable way to improve the DNN accuracy is increasing the training dataset size, which in turn can allow for more layers in the model. There might be potential in

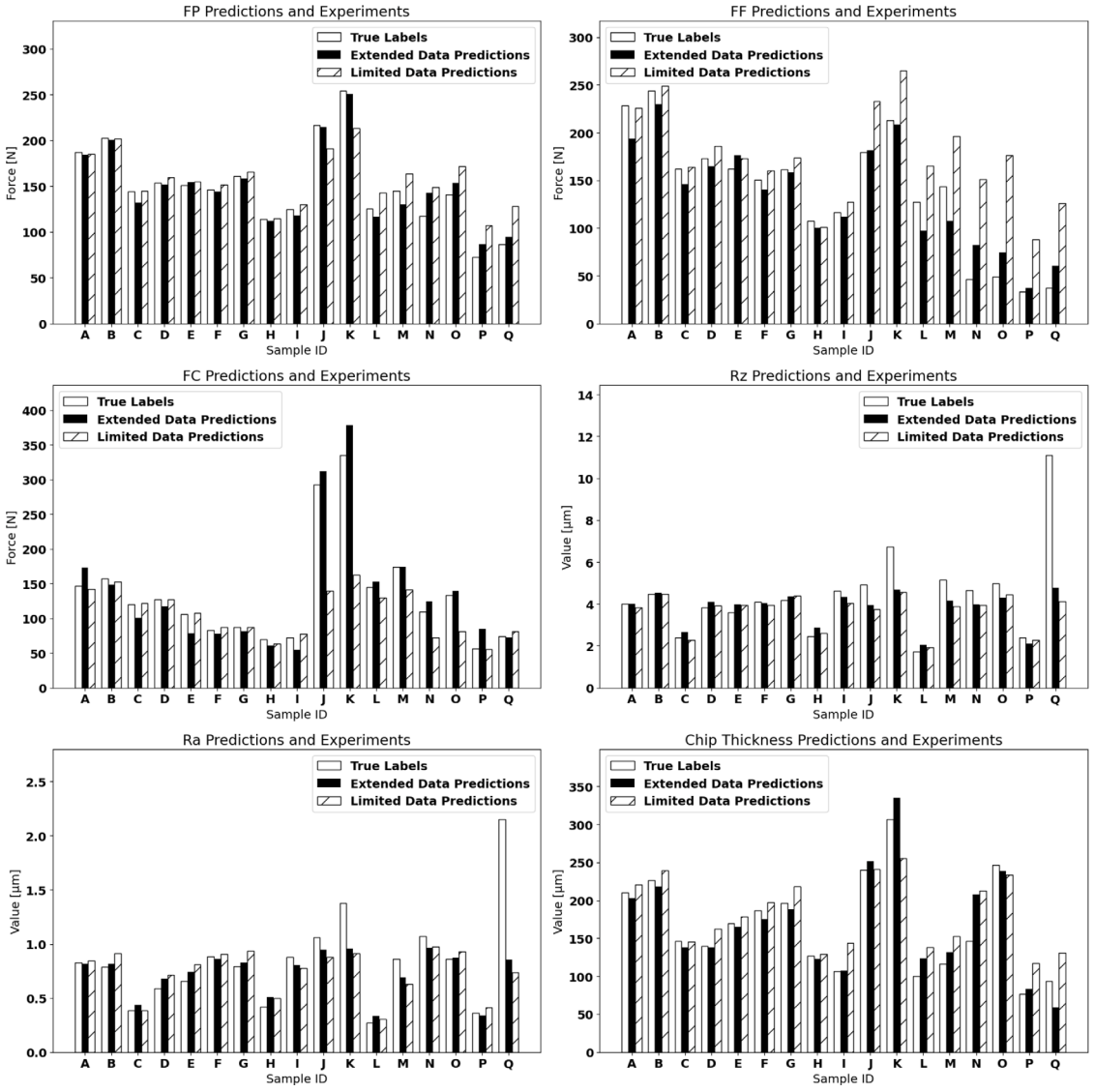

Fig. 11. The output of the DNN models compared to experimental results (True labels), extended data predictions include the FEM model results in the training dataset, limited data prediction has only experimental results.

Table 6
Prediction errors of the limited DNN model.

ID	F_P	F_f	F_C	R_z	R_a	t_c
A	1.22%	1.10%	2.90%	4.51%	1.95%	5.07%
B	0.36%	2.02%	3.11%	0.18%	15.53%	5.50%
C	0.41%	1.13%	1.23%	4.68%	1.27%	0.71%
D	3.68%	7.42%	0.26%	2.29%	20.70%	16.30%
E	2.53%	6.43%	1.55%	9.36%	23.53%	4.98%
F	3.33%	6.41%	5.31%	3.82%	1.99%	5.51%
G	2.87%	7.68%	0.04%	4.71%	18.01%	11.17%
H	0.55%	5.90%	8.58%	5.82%	18.92%	2.40%
I	3.99%	9.08%	6.63%	12.37%	11.78%	34.82%
J	11.96%	29.58%	52.26%	23.70%	17.26%	0.48%
K	16.21%	24.55%	51.49%	32.33%	33.79%	16.70%
L	13.61%	29.80%	10.39%	12.84%	11.71%	38.26%
M	12.79%	36.36%	18.95%	24.66%	26.79%	30.70%
N	26.91%	224.78%	34.39%	15.32%	9.34%	44.79%
O	22.10%	259.53%	39.13%	10.92%	8.26%	5.33%
P	47.96%	163.36%	0.90%	5.40%	14.84%	52.67%
Q	48.02%	238.05%	9.91%	62.96%	65.84%	40.44%

Table 7
Prediction errors of the hybrid FEML model.

ID	F_P	F_f	F_C	R_z	R_a	t_c
A	1.57%	15.16%	18.59%	0.00%	1.08%	3.25%
B	1.06%	5.94%	5.85%	1.45%	3.13%	3.61%
C	8.55%	9.93%	16.37%	11.32%	13.14%	5.88%
D	1.26%	4.83%	7.26%	6.62%	14.83%	1.11%
E	2.02%	8.39%	25.73%	10.44%	12.65%	2.96%
F	1.38%	6.94%	6.17%	1.41%	2.69%	5.83%
G	1.62%	1.91%	7.30%	4.16%	4.17%	4.09%
H	1.42%	6.54%	12.35%	15.74%	22.24%	3.16%
I	5.34%	3.94%	24.44%	6.12%	8.43%	0.62%
J	1.12%	0.75%	6.47%	19.92%	10.97%	4.71%
K	1.32%	1.97%	12.86%	30.40%	30.54%	9.11%
L	6.85%	23.73%	5.07%	19.40%	22.75%	23.33%
M	10.33%	25.38%	0.13%	19.26%	19.77%	13.06%
N	21.61%	76.75%	13.45%	14.61%	10.39%	41.75%
O	9.21%	52.29%	4.77%	13.56%	1.31%	3.35%
P	19.32%	10.03%	51.47%	12.36%	5.16%	8.90%
Q	9.21%	62.73%	1.78%	57.11%	60.28%	37.14%

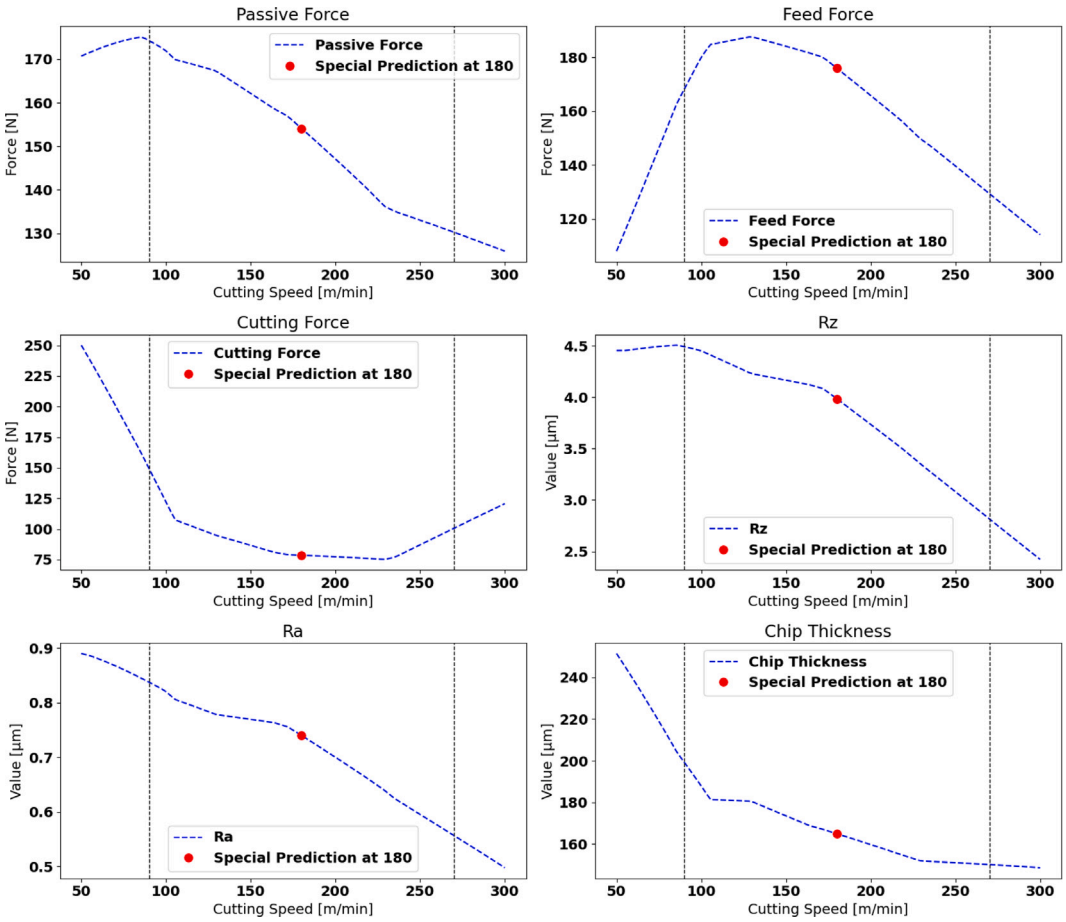

Fig. 12. Continuous interpolation of the DNN predicted process outputs as a function of cutting speed.

using higher order neurons, but that also has a risk of overfitting. The FEM model error is threefold, one source is the discretization error related to the meshing and linearization, another source is the time integration, and third most critical is the accuracy of the model data, which represents the material behaviour, friction, thermal aspect or other related phenomena. The first two can be reduced by decreasing the element size and time step, however these come with the cost of increased computational time. Improving the model data and material models is an active field of research which would not benefit from trying to discuss it here.

We created an additional prediction dataset from the hybrid FEML model to illustrate the model behaviour as a function of all the process parameters. Fig. 12 shows the model behaviour as a function of cutting speed. The cutting force components decrease with increasing cutting speed, complying with the theory and experiments [36,37]. The model behaviour outside the training data range (presented with the vertical dotted lines) shows instability commonly attributed to neural networks. The surface roughness values Rz and Ra decrease with increasing cutting speed, which is consistent with observations of machining other than stainless steels [38,39]. Daymi et al. [40] investigated the effect of cutting speed on chip morphology of Ti6Al4V. Their results show 20% decrease of chip thickness with increasing cutting speed from 50 m/min to 250 m/min. Our hybrid model prediction results show 18% decrease between the cutting speeds from 75 m/min to 275 m/min. Although the materials are not the same in the two studies, the behaviour is not uncommon.

The effect of feed on the model predictions is presented in Fig. 13. The cutting force components are nearly directly proportional to the feed, which is supported by the theory and experiments [41,42]. The change in the feed force near feed 0.15 mm/rev is caused by the tool protective chamfer, which is exactly 0.15 mm in length. When the feed approaches that value, the effective rake angle of the tool changes drastically and the cutting force components are distributed differently. The surface roughness is commonly known to increase with feed [43], which is predicted by the model as well [44]. Chip thickness is directly proportional to feed according to both established theory and our hybrid model.

The effect of cutting depth has directly proportional relationship with the cutting force components, as shown in Fig. 14. Cutting depth does not have universal effect on surface roughness, which is apparent in the model of theoretical surface roughness, in which only nose radius, minor cutting edge angle and feed are variables [43,45]. Cutting depth does have an effect however, e.g. with small cutting depths the chip formation moves towards the tool nose radius changing the force directions unfavourable for good surface finish or with very large cutting depths the tool deflection and potential vibrations, i.e. chatter, can cause poor surface finish. Experimental investigation by Murat et al. [46] shows increasing surface roughness with increasing feed above the typical levels in hard turning of AISI D2 cold working steel. The predictions of our hybrid model show only a small absolute difference in the surface roughness at different cutting depths, but the general trend appears to be that the roughness decreases with increasing cutting depth.

The temperature measurement setup needs improvement, because the formed chip interfered with the line of sight to the cutting insert rake face. Potential improvement is presented by Saez de Buruaga et al. [47], who measured the insert temperature from the tool side and calculated the tool-chip interface temperature with inverse methods.

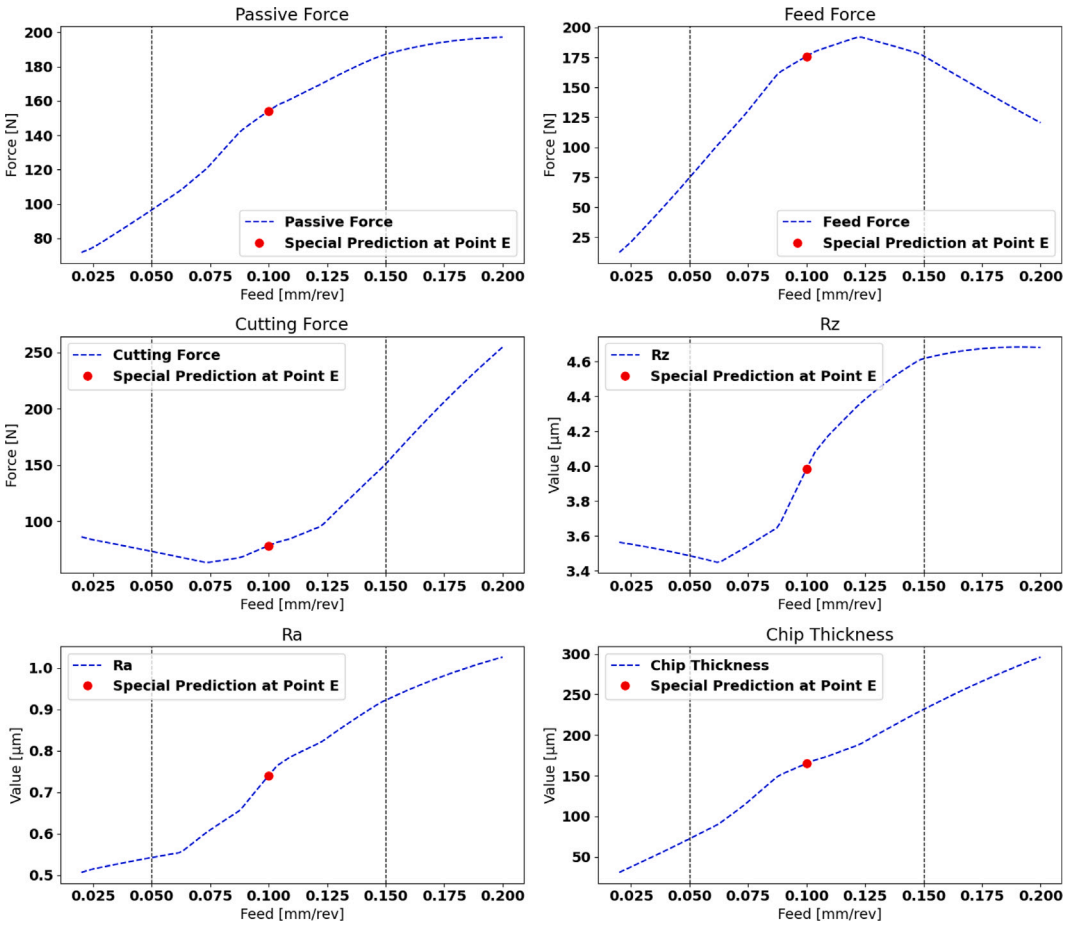

Fig. 13. Continuous interpolation of the DNN predicted process outputs as a function of cutting feed.

Their method is limited to semi-orthogonal case and requires a flat face on the insert side. Soler et al. [48] use an alternative method for IR camera calibration, by directly correlating the digital level and temperature of the measured surface. While this method improves the accuracy of the temperature measurement, this does not help to avoid the issue with blocked line of sight. The same paper shows a method to measure the rake face temperature by creating discontinuities on the workpiece, and this way removing the workpiece and the chip from the line of sight. This method is similar to what was by the author in Laakso [49], where the rake face temperature was measured directly after the tool-chip engagement ended. There are many temperature measurement techniques that are applicable in laboratory environment, but robust industrially relevant methods are missing, that can be used in everyday operations.

5. Conclusions

Our research investigated hybrid FEML model for turning of 42CrMo4 steel, using FEM model and machine learning. The hybrid model was successful in fulfilling the intended research outcomes, by reducing the need for experiments, reducing computational time and improving prediction accuracy by 10%. We made the following conclusions based on our results:

- Hybrid FEML model outperforms the ML model and FEM model independently.
- The prediction accuracy is good, 13% on average.
- Hybrid model required 50% less experimental data than ML model alone, and 45% less computing time than FEM model alone.
- Predicting and measuring surface roughness is more challenging than the other variables.
- Thermal imaging experiment setup needs further development to separate the radiation from workpiece, chips and insert.

These conclusions imply that the method has potential for general purpose predictive tool for turning operations in academic or industrial applications. The current model can predict the absolute values of surface roughness, cutting forces and chip thickness with acceptable accuracy, out of which the surface roughness is most beneficial for practical process design. In addition, the qualitative behaviour of the model agrees with existing research observations, at least within the training dataset range of operational parameters.

6. Limitations and future work

Further development of the model is needed especially regarding the prediction of the surface roughness, which in current model is entirely dependent on training with experimental data. Potential solutions for surface roughness prediction are voxel based material removal simulations, kinematic modelling, and regression models complemented with FEM results. Following that, tool wear effects need to be included in the model in addition to different work and insert materials. This can be achieved with more experimental results and FEM simulations for different materials. The current model is limited to turning operations and ductile or semi-ductile work materials. For milling, the DNN and FEM model need to be revised to accommodate different geometries and kinematics. Brittle materials can be implemented by using appropriate material models in FEM.

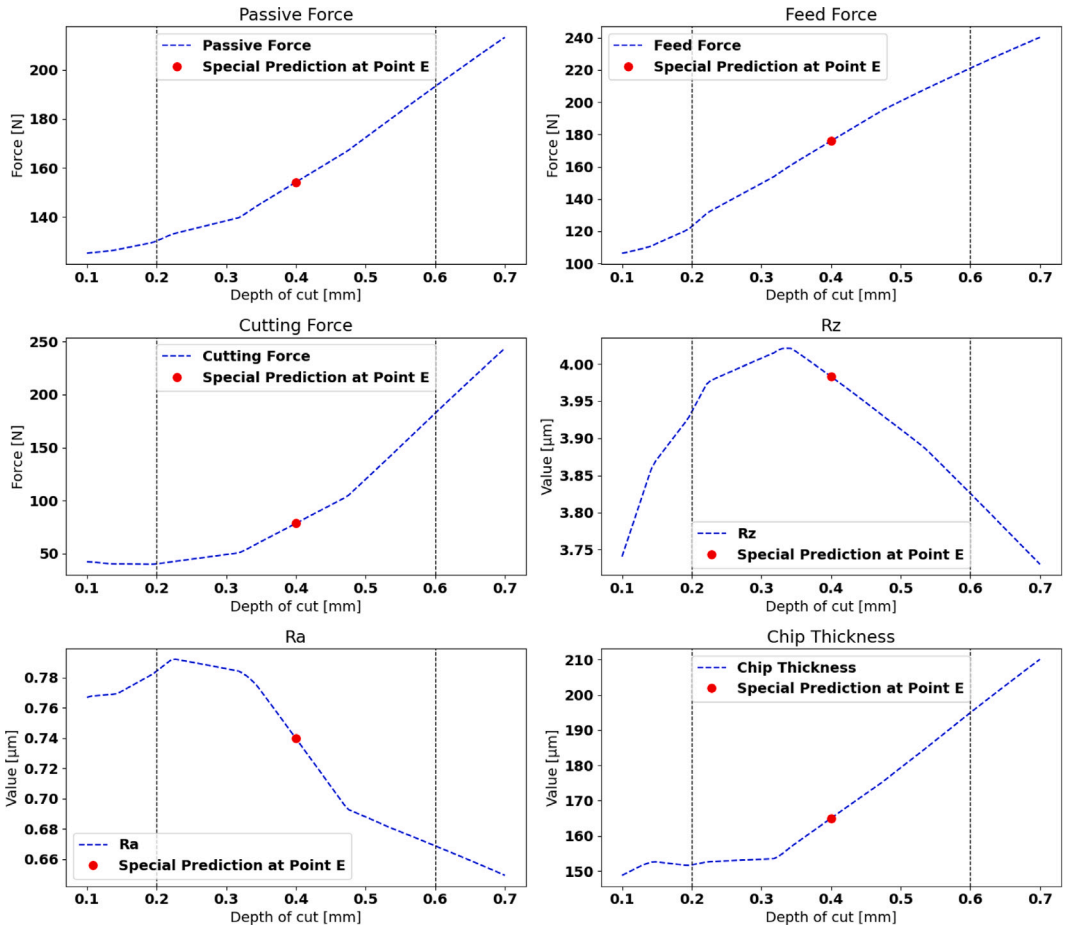

Fig. 14. Continuous interpolation of the DNN predicted process outputs as a function of cutting depth.

CRediT authorship contribution statement

Sampsa Vili Antero Laakso: Writing – review & editing, Writing – original draft, Visualization, Validation, Supervision, Software, Resources, Project administration, Methodology, Investigation, Funding acquisition, Formal analysis, Data curation, Conceptualization. **Andrey Mityakov:** Writing – review & editing, Visualization, Validation, Resources, Methodology, Investigation, Formal analysis, Data curation. **Tom Niinimäki:** Writing – original draft, Visualization, Validation, Methodology, Investigation, Formal analysis, Data curation. **Kandice Suane Barros Ribeiro:** Writing – review & editing, Validation, Supervision, Software, Resources, Project administration, Methodology, Funding acquisition. **Wallace Moreira Bessa:** Writing – review & editing, Validation, Supervision, Software, Resources, Project administration, Methodology, Funding acquisition.

Declaration of competing interest

The authors declare the following financial interests/personal relationships which may be considered as potential competing interests: Sampsa Laakso reports financial support was provided by Research Council of Finland. If there are other authors, they declare that they have no known competing financial interests or personal relationships that could have appeared to influence the work reported in this paper.

Acknowledgements

This research was done within Sustainable Materials and Manufacturing initiative (Susmat) in University of Turku funded by Research Council of Finland (grant nr. 352727). The authors would like to express our gratitude for Dr Thomas Björk and Ovako Imatra Oy Ab for guidance and for providing the experiment materials. The authors also wish to acknowledge CSC – IT Center for Science, Finland, for computational resources.

References

[1] R.H. Namlu, C. Turhan, B.L. Sadigh, S.E. Kılıç, Cutting force prediction in ultrasonic-assisted milling of Ti–6Al–4V with different machining conditions using artificial neural network, AI EDAM 35 (1) (2021) 37–48, http://dx.doi.org/10.1017/S0890060420000360.

[2] D. D'Addona, T. Segreto, A. Simeone, R. Teti, ANN tool wear modelling in the machining of nickel superalloy industrial products, CIRP J Manuf Sci Technol 4 (1) (2011) 33–37, http://dx.doi.org/10.1016/j.cirpj.2011.07.003.

[3] B. Das, S. Roy, R.N. Rai, S.C. Saha, Study on machinability of in situ Al–4.5%Cu–TiC metal matrix composite-surface finish, cutting force prediction using ANN, CIRP J Manuf Sci Technol 12 (2016) 67–78, http://dx.doi.org/10.1016/j.cirpj.2015.10.002.

[4] F. Ducobu, E. Rivière-Lorphèvre, E. Filippi, Application of the Coupled Eulerian-Lagrangian (CEL) method to the modeling of orthogonal cutting, Eur J Mech A Solids 59 (2016) 58–66, http://dx.doi.org/10.1016/j.euromechsol.2016.03.008.

[5] M. Agmell, V. Bushlya, S.V.A. Laakso, A. Ahadi, J.-E. Ståhl, Development of a simulation model to study tool loads in pcBN when machining AISI 316L, Int J Adv Manuf Technol (2018) http://dx.doi.org/10.1007/s00170-018-1673-y.

[6] M. Agmell, V. Bushlya, R. M'Saoubi, O. Gutnichenko, O. Zaporozhets, S.V.A. Laakso, J.-E. Ståhl, Investigation of mechanical and thermal loads in pcBN tooling during machining of Inconel 718, Int J Adv Manuf Technol (2020) http://dx.doi.org/10.1007/s00170-020-05081-8.

[7] Y.B. Guo, Q. Wen, A hybrid modeling approach to investigate chip morphology transition with the stagnation effect by cutting edge geometry, Society of Manufacturing Engineers, 2000.

[8] G. Markou, M. Papadrakakis, A simplified and efficient hybrid finite element model (HYMOD) for non-linear 3D simulation of RC structures, Eng Comput 32 (5) (2015) 1477–1524, http://dx.doi.org/10.1108/EC-11-2013-0269.

[9] A. Al-Qudsi, L. De Lorenzis, M. Scaraggi, A hybrid multiscale approach for rubber contact, Front Mech Eng 8 (2022) http://dx.doi.org/10.3389/fmech.2022.814607, Cited By :1.
[10] G.R. Bokil, Investigation and implementation of machine-learning-based hybrid material models (Master's thesis), Universitat Politècnica de Catalunya, 2022.
[11] F. Aldakheel, E.S. Elsayed, T.I. Zohdi, P. Wriggers, Efficient multiscale modeling of heterogeneous materials using deep neural networks, Comput Mech 72 (1) (2023) 155–171, http://dx.doi.org/10.1007/s00466-023-02324-9.
[12] F. Lerra, A. Candido, E. Liverani, A. Fortunato, Prediction of micro-scale forces in dry grinding process through a FEM—ML hybrid approach, Int J Precis Eng Manuf 23 (1) (2022) 15–29, http://dx.doi.org/10.1007/s12541-021-00601-2.
[13] X.P. Li, K. Iynkaran, A.Y.C. Nee, A hybrid machining simulator based on predictive machining theory and neural network modelling, J Mater Process Technol 89–90 (1999) 224–230, http://dx.doi.org/10.1016/S0924-0136(99)00068-0.
[14] I.S. Jawahir, X. Wang, Development of hybrid predictive models and optimization techniques for machining operations, J Mater Process Technol 185 (1) (2007) 46–59, http://dx.doi.org/10.1016/j.jmatprotec.2006.03.133.
[15] I.S. Jawahir, A.K. Balaji, K.E. Rouch, J.R. Baker, Towards integration of hybrid models for optimized machining performance in intelligent manufacturing systems, J Mater Process Technol 139 (1) (2003) 488–498, http://dx.doi.org/10.1016/S0924-0136(03)00525-9.
[16] C. Ahilan, S. Kumanan, N. Sivakumaran, J. Edwin Raja Dhas, Modeling and prediction of machining quality in CNC turning process using intelligent hybrid decision making tools, Appl Soft Comput 13 (3) (2013) 1543–1551, http://dx.doi.org/10.1016/j.asoc.2012.03.071.
[17] C. Pérez-Salinas, L.N.L. de Lacalle, A. del Olmo, C.S. Kumar, The relationship between the cutting-edge, tool wear, and chip formation during Inconel 718 dry cutting, Int J Adv Manuf Technol 132 (11) (2024) 6001–6017, http://dx.doi.org/10.1007/s00170-024-13685-7.
[18] X. Lazkano, P.X. Aristimuño, O. Aizpuru, P.J. Arrazola, Roughness maps to determine the optimum process window parameters in face milling, Int J Mech Sci 221 (2022) 107191, http://dx.doi.org/10.1016/j.ijmecsci.2022.107191.
[19] I. Aldekoa, A. del Olmo, L. Sastoque-Pinilla, S. Sendino-Mouliet, U. Lopez-Novoa, L.N.L. de Lacalle, Early detection of tool wear in electromechanical broaching machines by monitoring main stroke servomotors, Mech Syst Signal Process 204 (2023) 110773, http://dx.doi.org/10.1016/j.ymssp.2023.110773.
[20] J. Schoop, D. Adeniji, I. Brown, Computationally efficient, multi-domain hybrid modeling of surface integrity in machining and related thermomechanical finishing processes, in: 17th CIRP conference on modelling of machining operations, 17th CIRP CMMO, vol. 82, 2019, pp. 356–361, http://dx.doi.org/10.1016/j.procir.2019.03.225.
[21] J. Schoop, M. Hasan, H. Zannoun, Physics-informed and data-driven prediction of residual stress in three-dimensional machining, Exp Mech 62 (8) (2022) 1461–1474, http://dx.doi.org/10.1007/s11340-022-00880-4.
[22] B. Shi, A. Elsayed, A. Damir, H. Attia, R. M'Saoubi, A hybrid modeling approach for characterization and simulation of cryogenic machining of Ti–6Al–4V Alloy, J Manuf Sci Eng 141 (2) (2019) http://dx.doi.org/10.1115/1.4042307.
[23] A. Reimer, A cost effective approach to enhance surface integrity and fatigue life of precision milled forming and forging dies, 2019.
[24] S. Kurz, H. De Gersem, A. Galetzka, A. Klaedtke, M. Liebsch, D. Loukrezis, S. Russenschuck, M. Schmidt, Hybrid modeling: Towards the next level of scientific computing in engineering, J Math Ind 12 (1) (2022) 8, http://dx.doi.org/10.1186/s13362-022-00123-0.
[25] M. Hashemitaheri, S.M.R. Mekarthy, H. Cherukuri, Prediction of specific cutting forces and maximum tool temperatures in orthogonal machining by support vector and Gaussian process regression methods, Procedia Manuf 48 (2020) 1000–1008, http://dx.doi.org/10.1016/j.promfg.2020.05.139.
[26] B. Peng, T. Bergs, D. Schraknepper, F. Klocke, B. Döbbeler, A hybrid approach using machine learning to predict the cutting forces under consideration of the tool wear, Proc CIRP 82 (2019) 302–307, http://dx.doi.org/10.1016/j.procir.2019.04.031.
[27] M. Rosochowska, R. Balendra, K. Chodnikiewicz, Measurements of thermal contact conductance, J Mater Process Technol 135 (2) (2003) 204–210, http://dx.doi.org/10.1016/S0924-0136(02)00897-X.
[28] G.R. Johnson, W.H. Cook, A constitutive model and data for metals subjected to large strains, high strain rates and high temperatures, in: Proceedings of the 7th international symposium on ballistics, vol. 21, 1983, pp. 541–547.
[29] B. Stampfer, G. González, E. Segebade, M. Gerstenmeyer, V. Schulze, Material parameter optimization for orthogonal cutting simulations of AISI4140 at various tempering conditions, in: E. Govekar (Ed.), 18th CIRP conference on modeling of machining operations (CMMO), Ljubljana, Slovenia, June 15-17, 2021, 2021, p. 198, http://dx.doi.org/10.1016/j.procir.2021.09.034.
[30] T. Nguyen, A. Kashani, T. Ngo, S. Bordas, Deep neural network with high-order neuron for the prediction of foamed concrete strength, Comput-Aided Civ Infrastruct Eng 34 (4) (2019) 316–332, http://dx.doi.org/10.1111/mice.12422.
[31] M. Bagińska, P.E. Srokosz, The optimal ANN model for predicting bearing capacity of shallow foundations trained on scarce data, KSCE J Civ Eng 23 (1) (2019) 130–137, http://dx.doi.org/10.1007/s12205-018-2636-4.
[32] F. Pedregosa, G. Varoquaux, A. Gramfort, V. Michel, B. Thirion, O. Grisel, M. Blondel, P. Prettenhofer, R. Weiss, V. Dubourg, Scikit-learn: Machine learn-ing in python, J Mach Learn Res 12 (2011).
[33] F. Chollet, Deep learning with python, Manning, Shelter Island, 2018.
[34] L. Li, K. Jamieson, G. DeSalvo, A. Rostamizadeh, A. Talwalkar, Hyperband: A novel bandit-based approach to hyperparameter optimization, J Mach Learn Res 18 (185) (2018) 1–52.
[35] P.J. Huber, Robust estimation of a location parameter, Ann Math Stat 35 (1) (1964) 73–101, arXiv:2238020.
[36] H. Saglam, S. Yaldiz, F. Unsacar, The effect of tool geometry and cutting speed on main cutting force and tool tip temperature, Mater Des 28 (1) (2007) 101–111, http://dx.doi.org/10.1016/j.matdes.2005.05.015.
[37] G. Sutter, A. Molinari, Analysis of the cutting force components and friction in high speed machining, J Manuf Sci Eng 127 (2) (2005) 245–250, http://dx.doi.org/10.1115/1.1863253.
[38] A. Bhattacharya, S. Das, P. Majumder, A. Batish, Estimating the effect of cutting parameters on surface finish and power consumption during high speed machining of AISI 1045 steel using Taguchi design and ANOVA, Prod Eng 3 (1) (2009) 31–40, http://dx.doi.org/10.1007/s11740-008-0132-2.
[39] A. Hamdan, A.A.D. Sarhan, M. Hamdi, An optimization method of the machining parameters in high-speed machining of stainless steel using coated carbide tool for best surface finish, Int J Adv Manuf Technol 58 (1) (2012) 81–91, http://dx.doi.org/10.1007/s00170-011-3392-5.
[40] A. Daymi, M. Boujelbene, S.B. Salem, B.H. Sassi, S. Torbaty, Effect of the cutting speed on the chip morphology and the cutting forces, Arch Comput Mater Sci Surf Eng 1 (2) (2009) 77–83.
[41] W.B. Palmer, P.L.B. Oxley, Mechanics of orthogonal machining, Proc Inst Mech Eng 173 (1) (1959) 623–654, http://dx.doi.org/10.1243/PIMEPROC195917305302.
[42] U. Şeker, A. Kurt, İ. Çiftçi, The effect of feed rate on the cutting forces when machining with linear motion, J Mater Process Technol 146 (3) (2004) 403–407, http://dx.doi.org/10.1016/j.jmatprotec.2003.12.001.
[43] J.-E. Ståhl, M. Andersson, V. Bushlya, J. Zhou, C. Andersson, B. Högrelius, S. Gunnarsson, F. Schultheiss, Seco Tools AB, Metal cutting : Theories and models, Lund University Press, Division of Production and Materials Engineering, Lund University, Lund, Sweden, 2012.
[44] N.S. Kumar, A. Shetty, A. Shetty, A. K, H. Shetty, Effect of spindle speed and feed rate on surface roughness of carbon steels in CNC turning, Procedia Eng 38 (2012) 691–697, http://dx.doi.org/10.1016/j.proeng.2012.06.087.
[45] F. Schultheiss, S. Hägglund, V. Bushlya, J. Zhou, J.-E. Ståhl, Influence of the minimum chip thickness on the obtained surface roughness during turning operations, Proc CIRP 13 (2014) 67–71, http://dx.doi.org/10.1016/j.procir.2014.04.012.
[46] D. Murat, C. Ensarioglu, N. Gursakal, A. Oral, M.C. Cakir, Surface roughness analysis of greater cutting depths during hard turning, Mater Test 59 (9) (2017) 795–802, http://dx.doi.org/10.3139/120.111074.
[47] M. Saez-de-Buruaga, D. Soler, P.X. Aristimuño, J.A. Esnaola, P.J. Arrazola, Determining tool/chip temperatures from thermography measurements in metal cutting, Appl Therm Eng 145 (2018) 305–314, http://dx.doi.org/10.1016/j.applthermaleng.2018.09.051.
[48] D. Soler, P.X. Aristimuño, M. Saez-de-Buruaga, A. Garay, P.J. Arrazola, New calibration method to measure rake face temperature of the tool during dry orthogonal cutting using thermography, Appl Therm Eng 137 (2018) 74–82, http://dx.doi.org/10.1016/j.applthermaleng.2018.03.056.
[49] S.V.A. Laakso, Heat matters when matter heats – The effect of temperature-dependent material properties on metal cutting simulations, J Manuf Process 27 (2017) 261–275, http://dx.doi.org/10.1016/j.jmapro.2017.03.016.